Near-field FTIR Imaging: A Technique for Enhancing Spatial Resolution in FTIR Microscopy

JENNIFER J. SAHLIN,* and NIKOLAOS A. PEPPAS†

Polymer Science and Engineering Laboratories, School of Chemical Engineering, Purdue University, West Lafayette, Indiana 47907-1283

SYNOPSIS

Fourier transform infrared (FTIR) microscopy is a powerful analytical technique for characterization of polymeric materials. In certain applications, however, it would be advantageous to obtain higher spatial resolution than what is presently feasible. This contribution reviews the key principles of FTIR microscopy and presents a design enhancement that increases the spatial resolution that may be obtained with a standard FTIR microscope. Representative results are shown, which illustrate the technique's effectiveness. © 1997 John Wiley & Sons, Inc.

INTRODUCTION

The technique of Fourier transform infrared (FT IR) microscopy has been used extensively in analyzing polymer/polymer or solute/polymer diffusion.[1–6] Essentially, there are two key issues when using this technique: i.e., the general features of the device, and its major limitations. First, as presently designed, the IR microscope is very similar to an optical microscope; the optical paths for both the visible and IR radiation are identical through the sample plane. The operator can focus on specific features of the specimen, use the apertures to delineate the desired region, and subsequently collect the single beam IR spectrum for the sample. This spectrum is then ratioed to a background spectrum, which is collected through the same aperture.

As in all microscopy, there is a resolution limit dictated by diffraction effects. When two samples are less than 50 μm apart, they cannot be clearly resolved over the entire mid-IR range.[7] This means that when the spectrum of one sample is obtained, a certain amount of the energy from the second sample is being detected. Thus, pure spectra from each sample cannot be obtained.[7]

When light passes through a small aperture, the optical wave front spreads out, forming a series of bright and dark regions in the image plane. The diffraction pattern for a uniformly illuminated slit is given by the following:[8,9]

$$I_x = I_o \frac{\sin^2 x}{x^2} \tag{1}$$

where

$$x = \frac{\pi w \sin \theta}{\lambda} \tag{2}$$

In this expression, I_O is the maximum irradiance in the image, w is the slit width, and θ is the angular deviation from the pattern maximum. Figure 1 shows the relative intensity pattern as a function of position in the image plane. The relative amount of energy in each lobe is also shown.

In optical microscopy, it is the central lobe that defines the limit of resolution, since the human eye only distinguishes this central maximum. When the diffraction patterns from two neighboring point sources overlap, there is a separation distance at which the composite image clearly

* Present address: Process Technologies Laboratory, 3M Corporate Research Labs, 3M Center, Building 208-1-01, St. Paul, Minnesota 55101.

† To whom correspondence should be addressed.

Journal of Applied Polymer Science, Vol. 63, 103–110 (1997)
 CCC 0021-8995/97/010103-08

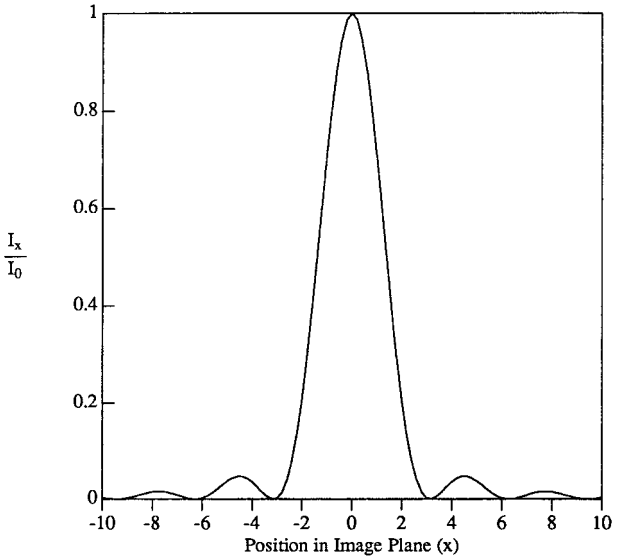

Figure 1 Relative light intensity as a function of position in the image plane. Distribution of energy: central maximum, 90.3%; secondary maxima, 4.7%; tertiary maxima, 1.7%.

shows that the two central lobes are overlapping. The two central maxima of the point sources that contribute to the composite image can be distinguished at this separation distance. Raleigh described this minimum separation distance as the position in the image plane at which the first minimum in the diffraction pattern occurs. For a slit aperture,[7] this is

$$d = \frac{0.5\lambda}{N_a} \tag{3}$$

where N_a is the numerical aperture of the optical system.

Although the human eye cannot detect the secondary lobes of overlapping diffraction patterns, these lobes contain spectral information, which is detected by the IR spectrometer's detector. Thus, these overlapping lobes result in a mixing of the two samples' spectral information. Furthermore, over three orders of magnitude in sample concentration are routinely measured with IR spectroscopy. Thus, the intensity of spectral features we wish to mask may be significantly larger than the feature we wish to measure.

The effect of the secondary lobes becomes important when examining small specimens. Apertures can be adjusted to mask a small specimen, but, due to diffraction effects at the aperture, the IR energy passes through the sample as a series of lobes. The outer lobes contain spectral information from the sample region beyond the desired area that had been delineated with the aperture. The stray light in the secondary lobes contaminates the spectra of small samples.

The energy in the diffraction pattern's secondary lobes that reaches the detector can be substantially reduced by using the technique of redundant aperturing. One essential feature that is required for this enhancement is that an on-axis. Cassegrain optical system be used below the specimen as a condenser. This optical geometry is essentially the same as for the objective lens. With this design, the lower aperture may be used to delineate the desired sample region. The upper aperture is then closed down to match the image of the lower aperture. This greatly reduces stray light from regions beyond the desired sample area by blocking the energy in the secondary lobes. Spectral purity is thus enhanced; the energy throughput, however, is substantially reduced.

The resolution of FTIR microscopy has been described as being primarily dictated by diffraction effects. One issue that has not been discussed in the literature is the fact that the actual dimensions of the remote aperture are substantially larger than their image in the sample plane. Thus, the aperture dimensions are much larger than the wavelength of the light impinging on them. The reduced image in the sample plane is the result of the Cassegrain objective and condenser; these lenses reduce the size of the image. Since these optics are diffraction-limited, diffraction effects are the main source of spectral impurity. Furthermore, slight deviations in the optical path alignment will reduce the colinearity of the energy through the instrument; this will also degrade the resolution. Since these are manually aligned, it may be a source of substantial variation in image quality for small sampling areas. The aperture dimensions also dictate the amount of energy impinging on the detector; thus, smaller aperture dimensions directly reduce the signal to noise, increasing the number of scans required to acquire good results.

Spectral purity can also be assured by closing the apertures down beyond the desired specimen area; the secondary lobes would now be sampling the desired specimen area. This over-aperturing technique substantially reduces the energy throughput. Thus, at some reduced slit size, insufficient energy is reaching the detector, and the technique fails.

This effect is readily apparent in Figure 2; this

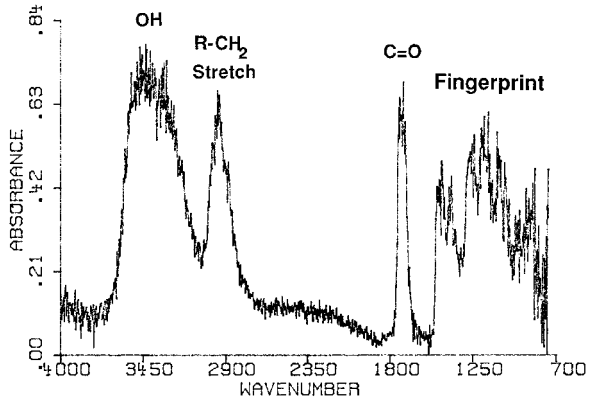

Figure 2 FTIR spectrum of a remotely apertured 4 μm thick PAA section containing 0.005 mol EGDMA/mol AA and EGDMA mounted on a BaF_2 crystal. Aperture: 5 $\times$ 180 μm; 4096 scans at 8 cm^{-1} resolution.

is a spectrum of a 4 μm thick section of poly(acrylic acid) (PAA). The slit dimensions delineated by dual aperturing are 5 $\times$ 180 μm. The single beam spectrum was ratioed to a background spectrum of the BaF_2 support. A total of 4096 scans was used to obtain this spectrum. Several key features, including the OH stretch and the carbonyl dimer stretch, are readily distinguished. The signal to noise level for the spectrum is not good, however; the region from 1800 to 400 cm^{-1} is uninterpretable. Since this is the region that can be used to positively identify the sample, it is imperative that this region is well resolved.

Thus, while FTIR microscopy is a substantial advancement in analytical techniques, it is limited by diffraction effects when the aperture dimensions in the image plane approach the wavelength of the light. In the mid-IR with dual-aperturing, this limitation reduces the resolution to about 15 μm.

IMPROVEMENTS MADE IN NEAR-FIELD FTIR MICROSCOPY TECHNIQUES

Experimental Difficulties

Near-field microscopy has been studied primarily as an advancement of optical microscopy; both theoretical[1,10,11] and experimental[1,2,12–16] results have been published. While most of these papers focused on visible wavelengths, the far-IR region was also studied. The fundamental ideas are, however, identical. Figure 3 shows three optically distinct regions surrounding an illuminated aperture. Each of these regions has unique dielectric properties, and each must be examined separately to determine the overall resolution limit of the system. A detailed analysis of this system was done by Betzig et al.[10] Essentially, light impinges upon an aperture (region I). The light that passes through the slit or pinhole becomes collimated due to the thickness of the aperture. When this light exits the aperture, it diffracts and spread out, forming an illumination cone. Generally, samples are studied in the far field (region III) of a microscope. In this regime, the resolution is limited by the wavelength of the light, since the radiation field from the sample contains structural information[11] for wavelengths larger than $\lambda/2$.

In the near-field (region II), on the other hand, the evanescent wave dictates the resolution since it contains structural information independent of the wavelength. However, the strength of the evanescent wave is an exponential function of the distance from the sample. Thus, the resolution limit in the near-field is dictated by two factors: the separation distance and the detector sensitivity; both of these parameters affect the minimum aperture size. Betzig et al.[10] found that for a slit aperture the minimum slit width was $\lambda/10$. The separation distance, which is on the order on nm in the visible spectrum, can be larger in the IR, since the wavelength of the light is larger.[10]

Most of the far-IR radiation impinging on the aperture plane does not pass through the aperture. Thus, since the separation distance between the aperture and the specimen can be less than

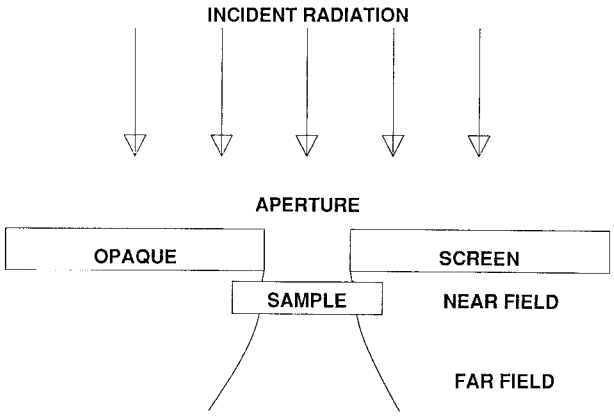

Figure 3 Schematic of the three optically distinct regions present when radiation impinges on an aperture:[11–16] I, incident radiation; II, near field; III, far field.

$\lambda/2$, concern may occur that sample heating may occur. Betzig et al.[10] addressed this question by investigating their assumption that the aperture screen is a perfect conductor. They found that this was a valid assumption as long as the aperture width and the screen thickness were larger than the extinction length of the radiation. For aluminum exposed to visible light, the extinction length is ~ 65 Å. Thus, sample heating effects should be minimal.

The only reported application of near-field techniques in conjunction with a standard FTIR microscope was by Messerschmidt.[7] The results included one spectrum of a polystyrene film. This sample had been physically masked with a 5 μm diameter aperture and was scanned 8000 times at 8 cm^{-1} resolution. This spectrum contained no stray light, whereas in a spectrum of a remotely apertured sample, stray light would have accounted for more than 50% of the signal.[3] Thus, Messerschmidt showed that IR spectra could be obtained with improved resolution. Furthermore, any contaminants that were next to the 5 μm spot would not contribute to the spectrum via stray light; thus, the resolution was dictated by the slit dimensions, and the secondary lobes of the diffraction pattern do not contribute to the measured spectrum. However, since the sample was physically masked, the sample cannot be moved in incremental steps relative to the aperture. Thus, the sample cannot be mapped; the mapping experiment is one of the major strengths of FTIR microscopy.

Near-field FTIR Imaging

Previous research clearly indicates that near-field techniques can be used to improve spectral resolution. Furthermore, mapping experiments can be done on specially designed optical systems. No previous work has been done to combine the mapping experiment and the near-field approach in conjunction with a FTIR spectrometer (model 800, Nicolet, Madison, WI). Figure 4 shows our design of a device that can be used to this end. This device mounts directly to the z-axis adjustment of the microscope (Spectra-Tech IR-PLAN, Stamford, CT). The turret supports an aperture arm, which extends across the mobile sample stage.

The aperture arm was initially designed out of aluminum. This design was sufficiently rigid to prevent the aperture from moving in the x,y plane when the sample was moved. The arm had to be redesigned out of flexible substrate, however, because of two major problems. First, there was significant variation in the thickness of the BaF_2 crystals, which served as specimen supports. Thus, the spacing between the aperture and the sample varied significantly and sometimes exceeded the critical separation for near-field studies. Furthermore, the controller of the motorized stage was prone to failure. This was a hardware problem in the stage controller and has recently been resolved by the manufacturer. In the context of these experiments, however, this hardware problem induced the stage to periodically raster to the end of its y coordinate. When this occurred, the aperture arm and the frame of the motorized stage collided, and the motor of the controller was overloaded.

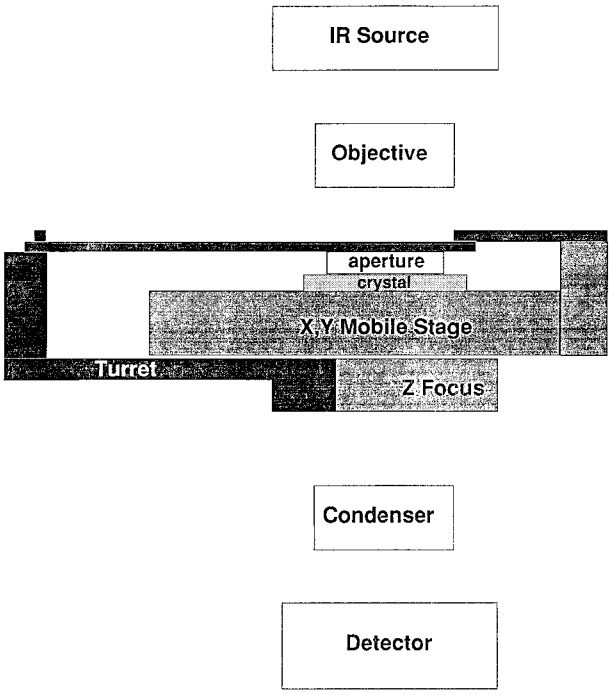

Figure 4 Diagram of the near-field aperture turret mounted on the z-focal adjustment of a FTIR microscope equipped with a motorized stage.

A flexible aperture arm minimizes these two problems. The separation distance between the aperture and the specimen can be adjusted by either counter-weighting the arm or by increasing the number of spacers built into it. Furthermore, when the stage controller fails, the aperture arm crumples. This minimizes the damage to the controller motor. The reduced tolerance between the aperture and the sample does, however, increase the torque on the arm when the stage moves in the

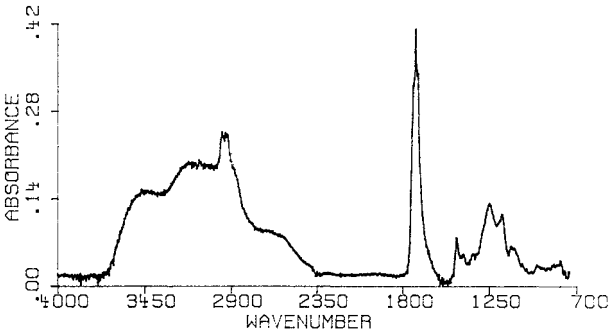

Figure 5 FTIR spectrum of a near-field apertured 2 μm thick PAA section containing 0.005 mol EGDMA/mol monomers mounted on a BaF_2 crystal. Aperture: 5 $\times$ 80 μm; 512 scans at 8 cm^{-1} resolution.

x,y plane. Thus, the arm was designed to extend beyond the front portion of the motorized stage; this extension can then be counterweighted or clamped in position.

Operationally, this near-field device increases the spatial resolution, which can be obtained during a mapping experiment; this enhanced resolution cannot be achieved with standard dual-masking techniques. The smaller sampling area does, however, increase the time required to run a mapping experiment. There are cases, however, when the increased resolution justifies its use. For example, this technique can be used to monitor the distribution of a drug within a hydrogel,[17] study inclusions within polymer blends, and investigate polymer–polymer diffusion.

RESULTS AND DISCUSSION

Improvements in FTIR Spectra Collection

Figure 5 shows a spectrum of a 4 μm thick section of poly(acrylic acid) (PAA) on a BaF_2 crystal. The PAA sample was produced *in situ* by polymerizing double distilled AA in 10% aqueous solution using sodium metabisulfite as an initiator and 0.5 mol % ethylene glycol dimethacrylate as a cross-linking agent. The aperture dimensions were 5 $\times$ 80 μm, the spectrum was collected at 8 cm^{-1} resolution, and the sample was scanned 512 times. When this spectrum is compared to that shown in Figure 2, it is clear that the new technique offers a substantial resolution enhancement. The reduction in stray light drastically improves the signal to noise. This reduces the number of scans required and also improves the clarity of the spectral details. The effect is most noticeable in the longer wavelengths (smaller wavenumbers) where diffraction effects have the most impact. For the aperture dimensions investigated, the number of scans was reduced by a factor of eight, while the aperture area was reduced by over a factor of two. Furthermore, since the sample sections are thin relative to the wavelength of the IR energy, the spatial resolution is dictated by the width of the slit in the near-field. In this instance, the spatial resolution was three times greater than is experimentally obtainable with dual-masking (15 μm).

FTIR Mapping Experiments

The ability to map compositional changes with enhanced spatial resolution was verified by monitoring the composition in a polymer laminate system. A polymer laminate was prepared by assembling together a first layer of PAA and a second layer of PAA loaded with poly(ethylene glycol) (PEG, $\bar{M}_n$ = 15,000). A detailed description of the polymer synthesis and sample preparation are given elsewhere.[18] Cryosectioning techniques were subsequently used to obtain a 2 μm thick cross section of the laminate. The polymer specimen was then lifted onto a BaF_2 crystal support during the sectioning process.

Typically, PEG was allowed to diffuse across the sample interface. Then, the concentration profile of the PEG in the PAA laminate was obtained by collecting a series of IR spectra. This experimental technique is similar to that presented by Klein and Briscoe[19] and is important in investigating polymer–polymer diffusion. Generally, the concentration profile that develops due to PEG diffusion is on the order of 10 μm or less. As a result, the enhanced spatial resolution feasible with the near-field approach is valuable. The polymer system investigated in this research exhibited unusually fast diffusion.

The BaF_2 crystal, which supported the thin laminate sections, was mounted on the motorized stage of an IR microscope. Small pieces of double-sided tape were used to secure the crystal; this prevented it from wiggling during the near-field experiment. The image of the sample was optimized by adjusting the lighting, the z-axis focus, and the condenser optics.[20] The lower optics were also set to account for the difference in refractive indices of the crystal and the sample. At this stage in the procedure, the interface between the two polymer layers was clearly visible in transmission mode. Subsequently, the BaF_2 crystal was rotated to align the sample's interface with the micro-

scope eyepiece's y-coordinate hash mark. The origin for the stage controller was then set to this position.

The motorized stage was rastered in the $-x$ direction until the bare BaF_2 crystal was positioned under the hash mark. The x controller position was then noted, and the stage was rezeroed. This set the new origin to the bare crystal's position and served as the background for the sample spectra. Thus, the previous origin position became the position of the sample's interface.

The near-field aperture arm was then positioned over the crystal, and the arm was counterweighted on both the front portion of the motorized stage and near the aperture position (see Fig. 4). This insured that the aperture was stationary and met the separation distance criterion for the near-field technique.

The subsequent alignment procedure was relatively delicate and laborious. The microscope was initially switched to reflectance mode, and the aperture slit was positioned over the eye-piece cross hair. This step required some adjustments of the z-axis focus. The microscope was then switched back to transmission mode and the iris, which controls the sample illumination, was opened wider since very little of the light could actually pass through the slit. If the aperture slit was not positioned properly along the y-coordinate, no light was visible. When this occurred, the aperture was adjusted in the y direction. The focus was then fine tuned, and the alignment in the x direction was rechecked. Since very little energy actually passed through the slit, it was essential to collect all of the transmitted energy. As a result, the condenser position was optimized for this new sampling configuration. This was first done with visible light; the alignment goal was to obtain the best visible definition of the slit, a symmetric rectangle.

When the visible alignment procedure was complete, the slit in the aperture was aligned directly under the eye-piece's y-hash mark, and the slit appeared as a uniform rectangle. Although both the z-focus and the condenser had been repositioned, the laminate's interface was still aligned with the hash mark. The defocusing of the optics relative to the sample caused the position of the interface to shift in the x-coordinate direction. Thus, a larger spectral region in this direction was scanned to insure both domains of the laminate are sampled sufficiently. For these experiments, the data were collected in 80 increments of 5 μm each. Thus, the data collection was initiated at -200 μm in the x direction from where the interface was when the background position was set.

All of the energy that passed through the near-field slit could be collected by delicately adjusting the condenser position. Only very slight changes were required if the system has been visibly optimized. The 2.5 mm diameter MCT-A microscope detector was filled with liquid nitrogen, and the system gain was increased to obtain an interferogram through the slit. The condenser position was then adjusted to maximize the interferogram. If the separation distance criterion was not met, the result was unsatisfactory. This was apparent in any spectrum that was collected under these conditions since the resultant spectrum was discontinuous over the frequency range. Another indicator of improper alignment that occasionally appeared was greater sample throughput than for the background. Reducing the separation distance and refocusing the microscope eliminated these problems.

When the system was properly aligned and tuned, the stage controller was used to collect

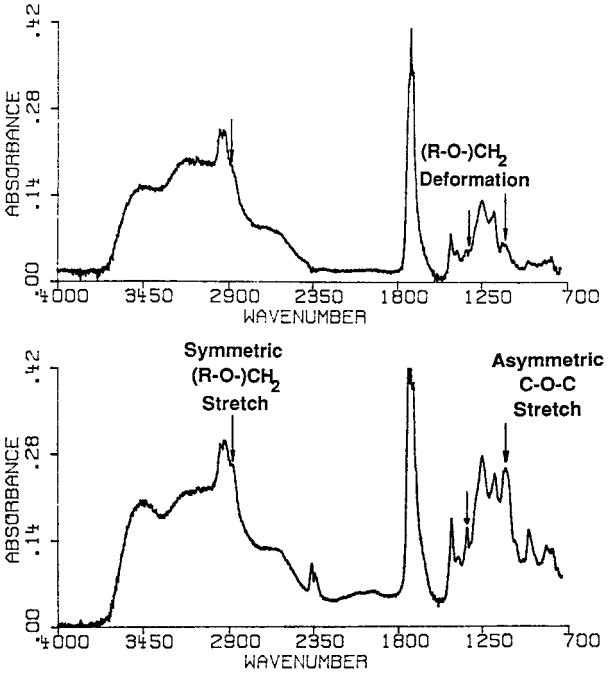

Figure 6 FTIR spectrum of a near-field apertured 2 μm thick PAA section containing of unloaded PAA containing 0.005 mol EGDMA/mol AA and EGDMA (top) and a PEG ($\bar{M}_n$ = 15,000 Da) loaded PAA network containing 0.005 mol EGDMA/mol AA and EGDMA (bottom). Aperture: 5 × 80 μm; 512 scans at 8 cm^{-1} resolution.

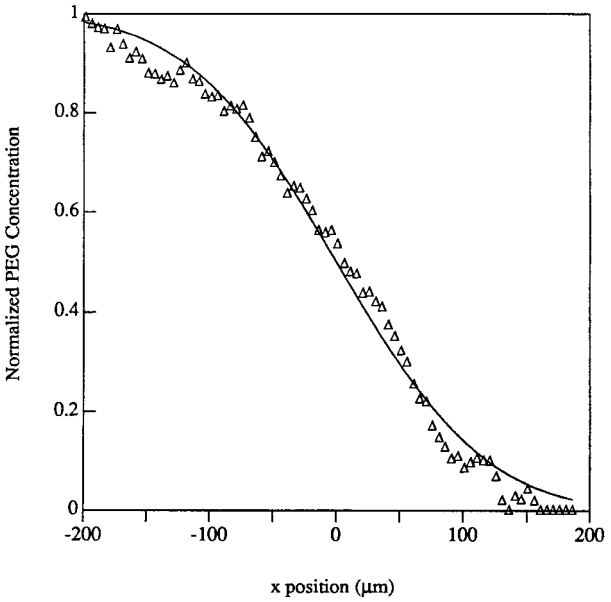

Figure 7 Normalized PEG ($\bar{M}_n$ = 15,000) concentration as a function of position. The PEG concentration was determined from the peak area of the asymmetric C—O—C stretch, 1130–1040 cm^{-1}. Contact time: 90 min: Aperture: 5 × 80 μm; 512 scans at 8 cm^{-1} resolution. Solid line: Fickian diffusion equation with $D = 8.1 \times 10^{-9}$ cm^2/s.

spectra of the background and of the sample. These mapping experiments required approximately six hours of collection time. This time requirement was due primarily to the number of scans collected for each position. Smooth peak shapes for integration were obtained by collecting 512 scans per spectrum. After the map spectra were collected, the area under the ether peak, from 1040 to 1130 cm^{-1}, was determined as a function of position. These data were then normalized with respect to the COC peak intensity. The number of scans required to obtain excellent qualitative results is substantially lower than 512.

Figure 6 is the near-field FTIR spectrum of a PEG-loaded PAA network. The ether stretch from 1130–1040 cm^{-1}, which is clearly discernible in the loaded sample's spectrum, will be used to map the concentration profile of PEG across the interface between the loaded and unloaded sections. The normalized PEG concentration as a function of position was fit to Fick's second law of diffusion by using nonlinear regression analysis. The data and the appropriate solution of Fick's second law are illustrated for data obtained from a representative mapping experiment in Figure 7. This figure clearly shows that near-field FTIR imaging experiments can be performed to evaluate compositional changes as a function of position within organic samples such as polymers.

CONCLUSIONS

The technique of near-field FTIR microscopy has been advanced by incorporating a stationary aperture within the optical path of a standard FTIR microscope. The aperture turret does not interfere with the x,y stage movement; this design can be utilized for near-field spectral mapping experiments. Thus, the compositional changes as a function of position can now be determined with enhanced spectral resolution.

The near-field technique easily increased the spatial resolution by a factor of three. Furthermore, the number of scans required to obtain quantitative results was reduced by over a factor of eight, while there was a concomitant reduction in total slit area of over a factor of two. The test cases examined in this study do not fully determine either the resolution limit of the experiment or the S/N enhancements, which can be achieved with this technique. Further detection and resolution gains can undoubtedly be obtained, especially with an optimized microscope detector.

While the aperture assembly used in this study was not highly sophisticated, the enhancements obtained were substantial. Future design modifications could control the separation distance between the aperture and the specimen more precisely and eliminate any potential aperture movement in the x,y plane.[20] Furthermore, a more powerful objective cassegrain would permit direct observation of the sample through the slit. This, in conjunction with a more tightly constrained separation distance between the aperture and the specimen, would minimize the shift due to refocusing the optics for the aperture. The refocusing process induces the sample to be shifted, as was discussed previously. One of the strengths of FTIR microscopy is that the sampling region can be visually inspected prior to the IR analysis. This would also be beneficial for experiments performed in the near-field.

The near-field FTIR imaging technique effectively enhances both the spatial resolution and the S/N of FTIR microscopy. Experimentally, this approach generally requires more alignment and data collection time. In selected applications, however, the gains are substantial.

This work was supported by Grant No. GM-45027 from the National Institutes of Health.

REFERENCES

1. E. Betzig, A. Lewis, A. Harootunian, M. Isaacson, and E. Kratschmer, *Biophys. J.,* **49,** 269–279 (1986).
2. G. A. Massey, J. A. Davis, S. M. Katnik, and E. Omon, *Appl. Opt.,* **24,** 1498–1501 (1985).
3. J. G. Van Alsten and S. R. Lustig, *Macromolecules,* **25,** 5069–5073 (1992).
4. J. G. Van Alsten, S. R. Lustig, and B. Hsiao, *Macromolecules,* **28,** 3672–3680 (1995).
5. E. Jabbari and N. A. Peppas, *Macromolecules,* **26,** 2175–2186 (1993).
6. E. Jabbari and N. A. Peppas, *J. Appl. Polym. Sci.,* **57,** 775–779 (1995).
7. R. G. Messerschmidt, in *The Design, Sample Handling, and Applications of Infrared Microscopes,* ASTM STP 949, P. B. Roush, Ed., American Society for Testing and Materials, Philadelphia, 1987, pp. 12–26.
8. R. G. Messerschmidt, in *Infrared Microspectroscopy: Theory and Applications,* R. G. Messerschmidt and M. A. Harthcock, Eds., Dekker, New York, 1988, pp. 1–19.
9. M. Young, *Optics and Lasers Including Fibers and Optical Waveguides,* 3rd. Rev. Ed., Springer-Verlag, New York, 1986, pp. 82–103.
10. E. Betzig, A. Harootunian, A. Lewis, and M. Isaacson, *Appl. Opt.,* **25,** 1890–1900 (1986).
11. U. Ch. Fischer and H. P. Zingsheim, *Appl. Phys. Lett.,* **40,** 195–197 (1982).
12. A. Harootunian, E. Betzig, M. Isaacson, and A. Lewis, *Appl. Phys. Lett.,* **49,** 674–677 (1986).
13. E. Betzig, M. Isaacson, and A. Lewis, *Appl. Phys. Lett.,* **51,** 2088–2090 (1987).
14. U. Ch. Fisher, *J. Vac. Sci. Technol. B.,* **3,** 386–390 (1985).
15. U. Ch. Fisher and H. P. Zingsheim, *J. Vac. Sci. Technol.,* **19,** 881–885 (1981).
16. D. W. Pohl, W. Denk, and M. Lanz, *Appl. Phys. Lett.,* **44,** 651–652 (1984).
17. M. T. amEnde and N. A. Peppas, *Pharm. Res.,* **12,** 2030–2035 (1995).
18. J. J. Sahlin and N. A. Peppas, *Macromolecules,* to appear.
19. J. Klein and B. J. Briscoe, *Nature,* **257,** 386–387 (1975).
20. N. B. Colthup, L. H. Daly, and S. E. Wiberley, *Introduction to Infrared and Raman Spectroscopy,* Academic Press, San Diego, 1990.

Received May 13, 1996
Accepted July 8, 1996